

Plane-strain discrete dislocation plasticity with climb-assisted glide motion of dislocations

This article has been downloaded from IOPscience. Please scroll down to see the full text article.

2013 Modelling Simul. Mater. Sci. Eng. 21 045008

(<http://iopscience.iop.org/0965-0393/21/4/045008>)

View [the table of contents for this issue](#), or go to the [journal homepage](#) for more

Download details:

IP Address: 131.111.7.9

The article was downloaded on 13/04/2013 at 10:37

Please note that [terms and conditions apply](#).

Plane-strain discrete dislocation plasticity with climb-assisted glide motion of dislocations

K Danas¹ and V S Deshpande²

¹ Laboratoire de Mécanique des Solides, C.N.R.S. UMR7649, Département de Mécanique, École Polytechnique, ParisTech, 91128 Palaiseau Cedex, France

² Centre for Micromechanics, Department of Engineering, University of Cambridge, Trumpington Street, Cambridge CB2 1PZ, UK

E-mail: kdanas@lms.polytechnique.fr and vsd@eng.cam.ac.uk

Received 13 November 2012, in final form 8 March 2013

Published 12 April 2013

Online at stacks.iop.org/MSMSE/21/045008

Abstract

A small-strain two-dimensional discrete dislocation plasticity (DDP) framework is developed wherein dislocation motion is caused by climb-assisted glide. The climb motion of the dislocations is assumed to be governed by a drag-type relation similar to the glide-only motion of dislocations: such a relation is valid when vacancy kinetics is either diffusion limited or sink limited. The DDP framework is employed to predict the effect of dislocation climb on the uniaxial tensile and pure bending response of single crystals. Under uniaxial tensile loading conditions, the ability of dislocations to bypass obstacles by climb results in a reduced dislocation density over a wide range of specimen sizes in the climb-assisted glide case compared to when dislocation motion is only by glide. A consequence is that, at least in a single slip situation, size effects due to dislocation starvation are reduced. By contrast, under pure bending loading conditions, the dislocation density is unaffected by dislocation climb as geometrically necessary dislocations (GNDs) dominate. However, climb enables the dislocations to arrange themselves into lower energy configurations which significantly reduces the predicted bending size effect as well as the amount of reverse plasticity observed during unloading. The results indicate that the intrinsic plasticity material length scale associated with GNDs is strongly affected by thermally activated processes and will be a function of temperature.

(Some figures may appear in colour only in the online journal)

1. Introduction

Over the last 25 years or so, computational solid mechanics has become an integral part of theoretical materials science. Significant attention has focused on mesoscale continuum mechanics where size matters. Such formulations are intermediate between a direct atomistic

simulations and an unstructured continuum description of deformation processes. A variety of theoretical frameworks are emerging to describe inelastic deformation at the mesoscale: in this study we shall focus on one of these methods, namely, discrete dislocation plasticity (DDP). In DDP, the dislocations are treated as line singularities in an elastic solid. A many body interaction problem involving the discrete dislocations needs to be solved together with a complimentary more conventional elasticity boundary value problem.

Following the pioneering work of Van der Giessen and Needleman [1], the DDP method has been shown to successfully predict numerous observations of plasticity size effects at the micrometre and sub-micrometre length scale. These include size effects in composites [2], bending [3], indentation [4], uniaxial compression [5], and under constrained shear [6]. The framework has also been used to investigate crack growth under monotonic [7] and fatigue loading [8]. Numerical methods to extend the framework to three-dimensional (3D) problems [9] and quasi-3D or the so-called 2.5D [10] have also been developed in order to capture essential features of plasticity including strain hardening under tensile loading. In all these studies the motion of dislocations is restricted to glide-only along specific slip planes, which is appropriate for deformations at temperatures significantly less than about $0.3T_m$ where T_m is the melting temperature of the metal. Diffusion is a significant mechanism of deformation at the temperatures encountered in many applications including for example the manufacture of semiconductor devices: the surface diffusion driven deformation of thin films leading to island formation, gives a possible means of producing quantum dots. It is thus of interest to extend the DDP framework to higher temperatures, where diffusion of vacancies affects the motion of dislocations.

Diffusion of vacancies permits dislocations to climb out of their slip planes. This is a potent relaxation mechanism: with the aid of small amounts of climb, dislocations can surmount small obstacles and thereby prevent the build-up of large pile-ups [11, 12]. In fact, recent experimental measurements of the uniaxial compression of indium micro-pillars at room temperature (room temperature is above $0.3T_m$ for Indium) by Lee *et al* [13] (see also [14]) revealed significantly smaller size effects compared with corresponding measurements for Gold [15], Ni and Ni₃Al [16] single crystals at room temperature. Moreover, a reduced indentation hardness size effect too has recently been reported by Franke *et al* [17] in copper as the temperature is increased from ambient to 200 °C. It is thus of considerable interest to extend the DDP framework to include the climb motion of dislocations.

Mordehai *et al* [18] have reported three-dimensional discrete dislocation calculations wherein climb motion of the dislocations is included in the form of a drag-type relation. This early study demonstrated the effect of climb in an infinite fcc crystal by investigating the activation of Bardeen–Herring sources. Other notable contributions which have incorporated climb into a discrete dislocation studies include the work by Xiang and Srolovitz [19] and Bakó *et al* [20]. However, to date a framework to solve boundary value problems in which the motion of discrete dislocations is by climb and glide has not yet been presented.

Here, we aim to develop a two-dimensional framework along the lines of the work of Van der Giessen and Needleman [1] that allows for the solution of boundary value problems with climb-assisted glide of dislocations. This would enable the investigation of the effect of climb on size effects in plasticity and make contact with the recent experimental observations referred to above.

The outline of the study is as follows. First we discuss the mechanisms and driving forces for the climb of edge dislocations and motivate a constitutive relation for the climb motion of these dislocations. Second, the two-dimensional (2D) DDP problem, with climb-assisted glide motion of dislocations, is formulated and discussed. Two boundary value problems are then solved using this formulation: (i) uniaxial tension and (ii) pure bending. Detailed results

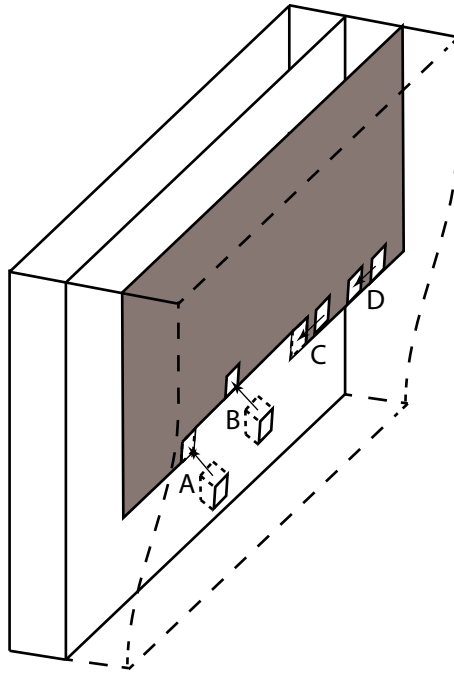


Figure 1. Sketch of the climb of an edge dislocation. The extra half-plane associated with the edge dislocation is shaded. At A, a vacancy from the crystal is destroyed directly at a jog. At B, a vacancy from the crystal jumps into the core. At C, an attached vacancy is destroyed at a jog. At D, an attached vacancy diffuses along the core.

are presented for the case of only one active slip system and then contrasted to the situation when three slip systems are active. Emphasis is given to the effect of the specimen size on the predicted responses.

2. Climb of edge dislocations

Figure 1 presents a simplified three-dimensional representation of the climb of an edge dislocation arising from the destruction of excess vacancies in the crystal. The jogs (steps in the edge of the extra half-plane of atoms) in the dislocation core are the sites where vacancies are created or permanently destroyed. Vacancies can reach a jog by either jumping directly into it or else by first jumping into the dislocation core and then diffusing along the core to a jog where they are destroyed. The elementary processes involved include (with reference to figure 1): (i) the jumping of a vacancy directly into a jog and its simultaneous destruction as at site A; (ii) the jumping of a vacancy into the core, where it becomes attached as at B; (iii) the destruction of an attached vacancy at a jog as at C and (iv) the diffusion of an attached vacancy along the core as at D. In many cases, vacancies are bound to the dislocation core by an attractive binding energy and diffuse along the dislocation more rapidly than in the crystal. Many more vacancies may therefore reach jogs by fast diffusion along the dislocation core than by diffusion directly into them through the crystal.

The jogs required for the climb process can be generated by the nucleation and growth of strings of attached excess vacancies along the core. When a string becomes long enough, it will collapse to produce a fully formed jog pair, as for example in the region bounded by

A and C in figure 1. The spacings between the jog pair then increase due to the continued destruction of excess vacancies at the jogs until a complete row of atoms has been stripped from the extra half-plane. In a two-dimensional view, the edge dislocation then climbs one atomic spacing; readers are referred to Ballufi *et al* [21] for a more detailed description of the climb of dislocations.

2.1. The equilibrium vacancy concentration

Gao and Cocks [22] have shown that in general there are three configurational forces acting on a dislocation to inhibit/promote climb. These are:

- (i) the climb component f_c of the Peach–Koehler force due to the elastic field of the dislocation,
- (ii) the so-called osmotic force f_o resulting from the change of free energy associated with the creation or destruction of vacancies due to the climb of the dislocations and
- (iii) a drag force on the dislocations due to the free energy of the vacancies associated with the evolution of the pressure field of the dislocation as it climbs.

The drag force is negligible compared with the other two forces [22] and hence is neglected in most analyses. In the treatment presented here we also adopt this approximation and only consider the f_c and f_o contributions to the configurational forces on the dislocation.

The osmotic force f_o per unit length on the edge dislocation is given in terms of the Boltzmann constant k and atomic vacancy volume Ω as [23]

$$f_o = \frac{kTb}{\Omega} \ln \left(\frac{c}{c_o} \right), \quad (1)$$

where c is the vacancy concentration in the vicinity of the dislocation with Burger's vector b and c_o is the standard-state concentration of vacancies (usually taken as the equilibrium concentration of vacancies in the absence of stress at the temperature T). Thus, the total climb force per unit length on the edge dislocation is

$$F = f_c + f_o = f_c + \frac{kTb}{\Omega} \ln \left(\frac{c}{c_o} \right). \quad (2)$$

If the dislocation is in climb equilibrium, $F = 0$ so that equation (2) yields the local equilibrium concentration of vacancies near the dislocation as

$$c_{\text{eq}} = c_o \exp \left(-\frac{f_c \Omega}{bkT} \right). \quad (3)$$

The inward vacancy current per unit dislocation length from the crystal into the dislocation core is proportional to the vacancy concentration in the vicinity of the dislocation and is given by $2\pi r_c K c_{\text{eq}}$ where r_c is the core radius and K a rate constant that depends on the core characteristics such as density of vacancy incorporation sites, diffusion rate of vacancies along the core and the binding energy of vacancies to the core. Under equilibrium conditions, the edge dislocation does not climb and thus this vacancy current into the core is balanced by an equal outward vacancy current from the dislocation core into the crystal.

2.2. Diffusion limited versus sink-limited climb kinetics

Vacancies are easily created or destroyed at jogs and hence they are maintained at their equilibrium value given by equation (3) in the immediate vicinity of jogs. If vacancies experience an attractive binding energy to the core and also diffuse relatively rapidly along it, a typical attached vacancy will diffuse a significantly large mean distance \bar{Z} , along the core

before it jumps back into the crystal. Each jog is therefore capable of maintaining the vacancy concentration essentially at equilibrium over a distance \bar{Z} along the dislocation core. Each jog, with the assistance of the two adjoining segments of high diffusivity core, therefore acts effectively as an ellipsoidal sink of semi-axes b and \bar{Z} having a surface on which the vacancy concentration is maintained in local equilibrium with the jog. The overall effectiveness of the dislocation as a sink then depends upon the magnitude of \bar{Z} and the mean spacing \bar{S} of jogs along the dislocation core. A wide range of dislocation sink efficiencies is thus possible. When $2\bar{Z}/\bar{S} \geq 1$, the effective jog sinks overlap along the dislocation line, which then acts as a highly effective line sink capable of maintaining local vacancy equilibrium everywhere along the dislocation line. The rate of vacancy destruction is limited only by the rate at which the vacancies can diffuse to the dislocation. The kinetics is therefore *diffusion limited*, and the dislocation is considered to be an ideal sink. Conditions that promote this situation are a high binding energy for attached vacancies, a relatively fast diffusion rate along the core, a small jog formation energy and a large vacancy supersaturation.

On the other hand, when fast diffusion of the attached vacancies to the jogs is impeded and \bar{Z} is therefore small (i.e. $\bar{Z} \approx b$), each jog acts as a small isolated spherical sink of radius b . If at the same time, \bar{S} is large, the jog sinks are far apart and the overall dislocation sink efficiency is relatively small. Under these conditions the rate of vacancy destruction will be limited by the rate at which the vacancies can be destroyed along the dislocation line. In the limit where the rate of destruction is slow enough so that it becomes essentially independent of the rate at which vacancies can be transported to the dislocation line over relatively long distances by diffusion and the kinetics are *sink limited*. The efficiency of the dislocation as a sink is then defined as

$$\eta = \frac{\text{flux rate at an actual sink}}{\text{flux rate at the corresponding ideal sink}}. \quad (4)$$

A dislocation that climbs rapidly enough so that ideal diffusion-limited conditions are achieved therefore operates with $\eta \rightarrow 1$. By contrast, a slowly acting dislocation sink has an efficiency approaching zero.

To illustrate these two limits we proceed to present an example of a spherical sink of radius r_c in an infinite medium. This example is chosen as it admits a simple analytical solution which displays all the essential features. The diffusion equation governing the concentration c of vacancies in the medium as a function of time t is

$$\frac{\partial c}{\partial t} = D\nabla^2 c = D \left(\frac{\partial^2 c}{\partial r^2} + \frac{2}{r} \frac{\partial c}{\partial r} \right), \quad (5)$$

where D is the diffusion coefficient and r is the radial distance measured from the centre of the spherical sink. The boundary and initial conditions are

$$c(r = r_c, t > 0) = \bar{c} \quad (6)$$

$$c(r \geq r_c, t = 0) = c_o, \quad (7)$$

$$c(r \rightarrow \infty, t \geq 0) = c_o. \quad (8)$$

The solution of equation (5) with the above initial and boundary conditions is

$$\frac{c - c_o}{\bar{c} - c_o} = \frac{r_c}{r} \left[1 - \operatorname{erf} \left(\frac{r - r_c}{2\sqrt{Dt}} \right) \right], \quad (9)$$

and the total vacancy current into the sink is then

$$I_v = 4\pi r_c^2 D \left. \frac{\partial c}{\partial r} \right|_{r=r_c} = 4\pi D r_c (c_o - \bar{c}) \left(1 + \frac{r_c}{2\sqrt{Dt}} \right). \quad (10)$$

The second term inside the bracket in the above equation is an initial transient that decays rapidly and becomes negligible when $2\sqrt{Dt} \gg r_c$ and for all practical purposes we can assume that the vacancy current is given by

$$I_v \approx 4\pi Dr_c(c_o - \bar{c}). \quad (11)$$

It now remains to determine the concentration \bar{c} that is maintained on the surface of the sink. This is governed by the kinetics of vacancies entering and leaving the sink. The vacancy current from the body into the sink is proportional to the concentration of vacancies in the vicinity of the sink and is hence given as $4\pi r_c^2 K \bar{c}$. The reverse current of vacancies out of the sink will equal the rate of transfer into the sink under equilibrium conditions, i.e. when the concentration of vacancies in the vicinity of the sink was equal to c_{eq} . Thus, the net rate of transfer of vacancies into the sink is given by

$$I'_v = 4\pi r_c^2 K (\bar{c} - c_{eq}). \quad (12)$$

In order to prevent a build-up of vacancies at $r = r_c$ the rate of transfer of vacancies by diffusion to the sink I_v should be equal to the net rate of vacancy transfer I'_v across $r = r_c$. Setting $I_v = I'_v$ and solving for \bar{c} gives

$$\bar{c} = \frac{Dc_o/(r_c K) + c_{eq}}{D/(r_c K) + 1}, \quad (13)$$

and the current into the sink follows as

$$I_v = \frac{4\pi Dr_c(c_o - c_{eq})}{1 + D/(Kr_c)}. \quad (14)$$

Thus, the sink efficiency is given by

$$\eta = \frac{1}{1 + D/(Kr_c)}. \quad (15)$$

When $D/(Kr_c) \ll 1$, $\bar{c} \approx c_{eq}$ and the kinetics is diffusion limited. At the other extreme, when $D/(Kr_c) \gg 1$, $\bar{c} \approx c_o$, i.e. the vacancy concentration is spatially uniform and the kinetics is sink limited.

2.3. Effect of the dislocation stress field

In the above treatment we do not take into account the effect of the dislocation stress field on the diffusivity of the vacancies. The diffusion equation, equation (5), is modified in the presence of the hydrostatic pressure p as

$$\frac{\partial c}{\partial t} = D\nabla^2 c + \frac{D\Omega'}{kT} \nabla \cdot (c\nabla p), \quad (16)$$

where Ω' is the relaxed vacancy volume. The additional term in the above equation is of importance only within a relatively small distance from the dislocation where $p\Omega'$ is of the order kT . Ham [24] has shown that the effect of this term after the decay of the initial transient in equation (10) can be approximated in a simple manner by making a relatively small change in the core radius r_c of the dislocations in equation (12). We thus argue that neglecting the stress term in the diffusion equation is a sufficiently accurate assumption for the present purposes.

2.4. A drag relation for edge dislocation climb

The computational framework for analysing the general case of mixed kinetics where $0 \leq \eta \leq 1$ is beyond the scope of this study. Rather, we develop a constitutive rule for the climb rate of

edge dislocations in the limit where the process is sink limited, i.e. $\eta \rightarrow 0$ or $D/(Kr_c) \gg 1$ and then compare it with the diffusion-limited case analysed by Hirth and Lothe [23].

Consider the two-dimensional boundary value problem where at time t there are N edge dislocations in the body with both glide and climb of the dislocations permitted. The body occupies a volume B and its boundary is denoted by ∂B . The equilibrium concentration of vacancies in the absence of dislocations at temperature T is c_0 . Given that vacancies are readily destroyed or created on the surface ∂B it is reasonable to assume that the vacancy concentration $c = c_0$ on ∂B at all times. As each dislocation climbs it either emits or absorbs vacancies and thereby each dislocation acts as a moving point source/sink in this two-dimensional setting. We have limited our consideration to the case where the kinetics is sink limited, i.e. the diffusion rate is fast compared with the rate of operation of the dislocation sources or sinks. Based on the analysis in section 2.2, we can thus assume that vacancy concentration $c = c_0$ throughout B at all times.

As described earlier, the vacancy current from the crystal into the dislocation core per unit line length of the edge dislocation is proportional to the vacancy concentration in the crystal and given as $2\pi r_c K c_0$. The reverse current of vacancies flowing from the dislocation core into the crystal will be the same as the rate of transfer from the crystal into the core under equilibrium conditions and hence given by $2\pi r_c K c_{eq}$. Thus, the net vacancy current into the dislocation core is

$$I_v = 2\pi r_c K (c_0 - c_{eq}) \quad (17)$$

and conservation of mass then gives the climb velocity v_c as

$$v_c = \frac{I\Omega}{b}. \quad (18)$$

Substituting for c_{eq} from equation (3) gives the climb rate as

$$v_c = \frac{2\pi\Omega r_c K c_0}{b} \left[1 - \exp\left(-\frac{f_c\Omega}{bkT}\right) \right]. \quad (19)$$

Under most circumstances it is reasonable to assume $|f_c\Omega| \ll |bkT|$ [23] so that equation (19) simplifies to

$$v_c = \frac{2\pi\Omega^2 r_c K c_0}{b^2 kT} f_c \equiv \frac{f_c}{B_c}, \quad (20)$$

where the climb drag coefficient is defined as

$$B_c \equiv \frac{b^2 kT}{2\pi\Omega^2 r_c K c_0}. \quad (21)$$

Hirth and Lothe [23] and Mordehai *et al* [18] considered the diffusion-limited case and assumed that the diffusion length of vacancies is given by the average dislocation spacing ℓ . With this assumption the dislocation climb law also takes the form $v_c = f_c/B_c$ with B_c given by

$$B_c = \frac{b^2 kT \ln(\ell/b)}{2\pi D c_0 \Omega^2}. \quad (22)$$

Thus, in this study we shall use B_c as a parameter to investigate the effect of climb with the results being equally valid in both the sink-limited kinetic and diffusion-limited kinetic limits.

3. Modelling dislocation climb with discrete dislocation dynamics

The two-dimensional (2D) plane strain, small-strain DDP framework wherein dislocation motion occurs both by climb and glide is described in this section with an emphasis on the

differences with the glide-only formulation of Van der Giessen and Needleman [1]. In DDP, the dislocations are treated as line defects in an otherwise elastic continuum. In this plane-strain formulation the edge dislocations lie in the x_1 - x_2 plane. At each stage of loading, the stress and deformation state is computed using superposition [1] of a singular field ($\tilde{\cdot}$) and a smooth image field ($\hat{\cdot}$) that enforces the boundary conditions. When dislocations can move only by glide, the deformation state of the body can be computed from the current positions of dislocations including those that have exited the domain and left behind slip steps. When the motion of the dislocations is by a combination of glide and climb, the deformation state of the body cannot be constructed from only the knowledge of the current positions of the dislocations. Thus, it is numerically more convenient to write the problem in rate or an incremental form and update the deformation of the body during each increment of the dislocation motion.

At time t , the body contains N edge dislocations moving with a velocity $v_i^{(I)}$, where $I = 1, \dots, N$. The change in position of dislocation I gives rise to a displacement field $\tilde{u}_i^{(I)}(x_j)$ at each material point x_j within the body. The total displacement rate is written as the superposition

$$\dot{u}_i(x_j, t) = \dot{\hat{u}}_i(x_j, t) + \dot{\tilde{u}}_i(x_j, t), \quad (23)$$

where x_j denotes the position of a material point and

$$\dot{\tilde{u}}_i(x_j, t) = \sum_{I=1}^N \dot{\tilde{u}}_i^{(I)}. \quad (24)$$

We typically calculate $\dot{\tilde{u}}_i^{(I)}$ from time t to time $t + \Delta t$ using a finite difference scheme as described subsequently.

The computation of the deformation history is carried out in an incremental manner. Each time step involves three main computational stages: (i) determining the climb and glide Peach–Koehler forces on the dislocations; (ii) determining the rate of change of the dislocation structure, caused by the motion of dislocations, generation of new dislocations, their mutual annihilation or exit from the domain and their possible pinning and release from obstacles; and (iii) determining the stress and strain state for the updated dislocation arrangement.

At a given stage of loading, the material velocity, strain rate and stress-rate fields are written as the superposition of two fields

$$\dot{u}_i = \dot{\hat{u}}_i + \dot{\tilde{u}}_i, \quad \dot{\epsilon}_{ij} = \dot{\hat{\epsilon}}_{ij} + \dot{\tilde{\epsilon}}_{ij}, \quad \dot{\sigma}_{ij} = \dot{\hat{\sigma}}_{ij} + \dot{\tilde{\sigma}}_{ij}, \quad (25)$$

where the ($\tilde{\cdot}$) fields are the sum of all the individual dislocations, namely,

$$\dot{\tilde{u}}_i = \sum_{I=1}^N \dot{\tilde{u}}_i^{(I)}, \quad \dot{\tilde{\epsilon}}_{ij} = \sum_{I=1}^N \dot{\tilde{\epsilon}}_{ij}^{(I)}, \quad \dot{\tilde{\sigma}}_{ij} = \sum_{I=1}^N \dot{\tilde{\sigma}}_{ij}^{(I)}. \quad (26)$$

These ($\tilde{\cdot}$) fields give rise to traction rates $\dot{\tilde{T}}_i$ and material velocities $\dot{\tilde{U}}_i$ on the boundary of the body. With body forces neglected, the principle of virtual work takes the form

$$\int_V \sigma_{ij} \delta \hat{\epsilon}_{ij} dV = \int_{S_T} T_i \delta \hat{u}_i dS, \quad (27)$$

where V is the volume of the body analysed and S_T is the external surface over which traction boundary conditions are imposed. Substituting σ_{ij} from equation (25)₃ (which is true in both total and rate form), and then carrying out integration by parts and the divergence theorem in equation (27), one readily obtains

$$\int_V \hat{\sigma}_{ij} \delta \hat{\epsilon}_{ij} dV = \int_{S_T} (T_i - \tilde{T}_i) \delta \hat{u}_i dS. \quad (28)$$

At time t the stress field and the current positions of all the dislocations are known. An increment of loading is prescribed and the dislocation structure updated to time $t + \Delta t$, such that $\hat{\sigma}^{(t+\Delta t)} = \hat{\sigma}^{(t)} + \dot{\hat{\sigma}} \Delta t$. The rate boundary value problem is then given as

$$\Delta t \int_V \dot{\hat{\sigma}}_{ij} \delta \hat{\epsilon}_{ij} dV = \int_{S_T} \left(T_i^{(t+\Delta t)} - \tilde{T}_i^{(t+\Delta t)} \right) \delta \hat{u}_i dS - \int_V \hat{\sigma}_{ij}^{(t)} \delta \hat{\epsilon}_{ij} dV, \quad (29)$$

which can be conveniently solved for the ($\hat{\cdot}$) fields using the prescribed traction and displacement boundary conditions on S_T and S_u , respectively, by a finite element (FE) analysis.

3.1. Dislocation interaction constitutive rules

Attention is restricted to elastically isotropic and homogeneous crystals with Young's modulus E and Poisson's ratio ν . Constitutive rules for 2D dislocation dynamics were given by Kubin *et al* [25] and subsequently employed by Van der Giessen and Needleman [1] in plane-strain analyses. We summarize the plane-strain rules, highlighting the differences that arise due to dislocation climb.

The main difference is that with dislocation climb permitted, dislocations are no longer confined to a fixed slip plane as they can climb out of that plane. Hence, the basic entity is a slip system (i.e. the orientation in the lattice of the slip plane normal and the slip direction) rather than a slip plane. The glide and climb force work conjugates to infinitesimal variations of the position of dislocation I (i.e. the glide and climb Peach–Koehler force) are given by

$$f_g^{(I)} = \left(\hat{\sigma}_{ij} + \sum_{J \neq I} \tilde{\sigma}_{ij}^{(J)} \right) b_j^{(I)} m_i, \quad (30)$$

$$f_c^{(I)} = - \left(\hat{\sigma}_{ij} + \sum_{J \neq I} \tilde{\sigma}_{ij}^{(J)} \right) b_j^{(I)} s_i, \quad (31)$$

respectively, where $b_j^{(I)}$ is Burger's vector of dislocation I residing on a slip system with unit normal m_i and a unit vector s_i in the slip direction such that $e_{ijk} s_j m_k$ is a unit vector in the x_3 direction (e_{ijk} is the permutation tensor). The glide velocity of dislocation I is given by the usual drag relation [1]

$$V_g^{(I)} = \frac{f_g^{(I)}}{B_g}, \quad (32)$$

where B_g is the drag coefficient in glide while the analysis of section 2.4 gives a drag relation for the climb velocity of the form

$$V_c^{(I)} = \frac{f_c^{(I)}}{B_c}. \quad (33)$$

In the calculations presented subsequently, we shall use B_c as a parameter to investigate the effect of climb.

New dislocation pairs are generated by simulating Frank-read sources. In two dimensions, this is mimicked by discrete point sources on a slip system which generate a dislocation dipole with their Burger's vector aligned with s_i . This occurs when the magnitude of the Peach–Koehler force at that source exceeds a critical value $\tau_{\text{nuc}} b$, where b is the magnitude of Burger's vector for a time period t_{nuc} . The distance L_{nuc} between the dislocations of the nucleated dipole is taken to be specified by

$$L_{\text{nuc}} = \frac{E}{4\pi(1-\nu^2)} \frac{b}{\tau_{\text{nuc}}}, \quad (34)$$

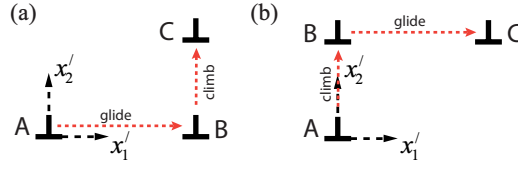


Figure 2. Sketch of the combined glide and climb of an edge dislocation during its motion from location A to location C. In (a) the dislocation moves from A to C by first gliding to the intermediate location B and then climbing to C while in (b) the motion involves first climbing to the intermediate location B and then gliding to the final position C. The local axes attached to the dislocation x_1' and x_2' are also illustrated.

such that the dislocation source and the two nucleated dislocations are all co-linear (i.e. we neglect climb of the nascent dislocation loop). This choice of L_{nuc} ensures that the shear stress of one dislocation acting on the other is balanced by the slip system shear stress τ_{nuc} . Annihilation of two opposite signed dislocations on the same slip system occurs when they are sufficiently close together. This is modelled by eliminating the dislocations when they are within a material-dependent critical annihilation distance L_e . Note that unlike in the glide-only formulation where only opposite signed dislocations on a given slip plane can annihilate each other, in this formulation opposite signed dislocations on a given slip system can annihilate each other. Thus, annihilation of two opposite signed dislocations on a particular slip system occurs when they are within a radius L_e irrespective of their current slip plane.

Obstacles to dislocation motion are modelled as points associated with a slip system. Dislocations on the obstacle slip system get pinned as they try to pass through that point. Again, unlike in the only-glide deformation case, dislocations and obstacles are associated with slip system rather than a slip plane. Thus, dislocations on the obstacle slip system that pass within a specified distance, taken to be L_e , get pinned to that obstacle. Pinned dislocations can only pass through an obstacle when their Peach–Koehler force exceeds an obstacle dependent value $\tau_{\text{obs}}b$.

3.2. Calculation of the ($\tilde{\cdot}$) velocity fields

The calculation of the \tilde{u}_i is complicated by the fact that dislocation motion is by a combination of glide and climb as illustrated in figure 2. The complication arises due to the fact that while the stress and strain fields associated with a dislocation (i.e. the $\tilde{\sigma}_{ij}$ and $\tilde{\epsilon}_{ij}$) are unique, the corresponding displacement field \tilde{u}_i depends on the history of motion. To clarify, consider a perfect crystal and consider two limiting processes by which an edge dislocation may be inserted into this crystal: (i) insert the dislocation into the crystal by a pure glide process as shown in figure 3(a) wherein the motion of the edge dislocation is along the direction of Burger's vector and (ii) insert the extra half-plane by a climb-like process wherein the motion of the dislocation is perpendicular to the direction of Burger's vector as shown in figure 3(b). The resultant displacement fields (in an infinite crystal) due to these two processes are given by

$$\tilde{u}_1 = \frac{b'}{2\pi(1-\nu)} \left[\frac{x_1'x_2'}{2(x_1'^2 + x_2'^2)} - (1-\nu) \tan^{-1} \left(\frac{x_1'}{x_2'} \right) \right], \quad (35)$$

$$\tilde{u}_2 = \frac{b'}{2\pi(1-\nu)} \left[\frac{x_2'^2}{2(x_1'^2 + x_2'^2)} - \frac{(1-2\nu)}{4} \ln \left(\frac{x_1'^2 + x_2'^2}{b^2} \right) \right] \quad (36)$$

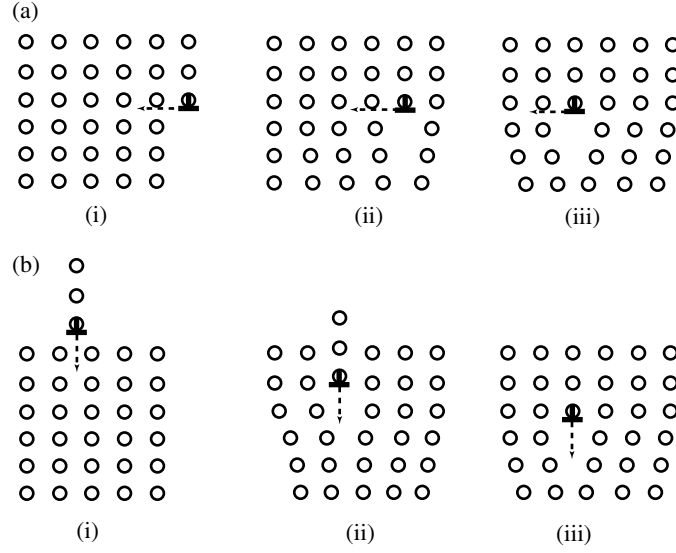


Figure 3. Sketch illustrating the two limiting processes to insert an edge dislocation into a perfect crystal: (a) a pure glide process wherein the dislocation motion is along the direction of Burger's vector and (b) a climb-like process wherein the motion of the dislocation is perpendicular to Burger's vector.

for the glide process sketched in figure 3(a) and by

$$\check{u}_1 = \frac{b'}{2\pi(1-\nu)} \left[\frac{x'_1 x'_2}{2(x_1'^2 + x_2'^2)} + (1-\nu) \tan^{-1} \left(\frac{x'_2}{x'_1} \right) \right], \quad (37)$$

$$\check{u}_2 = \frac{b'}{2\pi(1-\nu)} \left[\frac{x_2'^2}{2(x_1'^2 + x_2'^2)} - \frac{(1-2\nu)}{4} \ln \left(\frac{x_1'^2 + x_2'^2}{b^2} \right) \right]. \quad (38)$$

for the climb-like process sketched in figure 3(b). Here x'_1 and x'_2 are the coordinates of the material point at which the displacement is being calculated as measured in the local coordinate system of the edge dislocation as shown in figure 2 and b' is the signed magnitude of Burger's vector.

Now consider the motion of the edge dislocation from location A at time t to location C at time $t + \Delta t$ involving glide and climb; see figure 2. We decompose this motion into glide-only and climb-only components, as shown in figure 2(a), where location B is the intermediate location of the dislocation after it has completed its glide-only part of its motion at time $t + \Delta t_g$. We then calculate the displacement rate $\dot{\check{u}}_i^{(I)}$ due to the motion of the dislocation (I) from A to C as

$$\dot{\check{u}}_i^{(I)} = \frac{1}{\Delta t} \left[\bar{u}_i^{(t+\Delta t_g)} - \bar{u}_i^{(t)} + \check{u}_i^{(t+\Delta t)} - \check{u}_i^{(t+\Delta t_g)} \right]. \quad (39)$$

If the situation as shown in figure 2(b) occurs, i.e. the motion of the edge dislocation from A to C occurs by first a climb step followed by a glide step, then equation (39) needs to be modified by swapping the order of the \bar{u}_i and \check{u}_i terms.

In the procedure described above, we decompose the motion of the dislocation into glide-only and climb-only segments. The displacement rate $\dot{\check{u}}_i$ will depend on the order to these two events, i.e. whether the glide-only segment precedes the climb-only segment or vice versa as

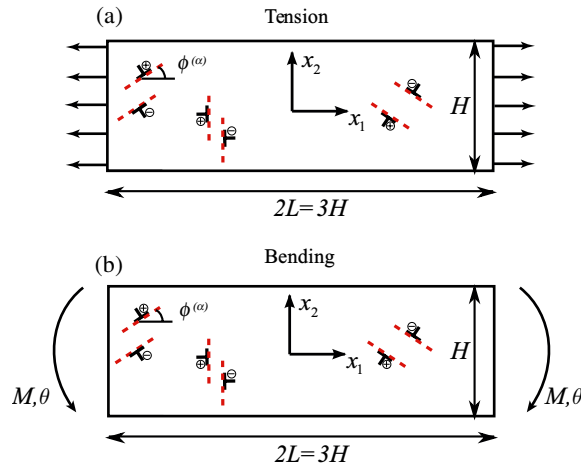


Figure 4. Sketch of the single crystal specimen analysed. The sign convention for the dislocations along with the leading specimen dimensions and the co-ordinate system employed are marked. Two boundary value problems are analysed (a) uniaxial tension in the x_1 direction and (b) pure bending about the x_1 -axis.

shown in figures 2(a) and (b). Within a time step Δt , we cannot resolve the order of these events and hence need to arbitrarily assume the glide and climb sequence within a time step. This is done using the following reasoning. Recall that in discrete dislocation dynamics, we employ an explicit time integration scheme. A consequence of this integration scheme is that there is some vibratory motion of dislocations that may be a numerical artifact. We ensure that these vibratory motions do not give any net contribution to the \tilde{u}_i fields by employing the following ‘sign-convention’: the glide-only segment precedes the climb-only segment when an edge dislocation is gliding along the positive s_i direction and vice versa. This convention ensures no net contribution to \tilde{u}_i due to purely vibratory motion of the dislocations.

3.3. The boundary value problems

We illustrate the effect of climb on the response of single crystals using two illustrative examples: (i) uniaxial tension and (ii) pure bending as sketched in figure 4. Consider a single crystal of length $2L$ and width H with slip systems orientated at angles $\phi^{(\alpha)}$ with respect to the x_1 -axis, where α is the slip system designation. Uniaxial tension is imposed by prescribing a displacement rate \dot{U} (see figure 4(a)) such that

$$\dot{u}_1 = \pm \dot{U}, \quad \text{and} \quad \dot{T}_2 = 0 \quad (40)$$

on $x_1 = -L$ and $x_1 = L$, respectively, as well as free surface conditions on the top and bottom surfaces, i.e. $\dot{T}_1 = \dot{T}_2 = 0$ on $x_2 = -H/2$ and $x_2 = H/2$. In addition we impose $\dot{u}_2 = 0$ on the corner $(x_1, x_2) = (-L, -H/2)$ in order to prevent rigid body motion in the x_2 direction. In all the calculations a loading rate $\dot{U}/L = 1000 \text{ s}^{-1}$ is employed.

Pure bending on the crystals is imposed by specifying displacements (see figure 4(b))

$$\dot{u}_1 = \pm \dot{\theta}(x_2 - x_0) \quad (41)$$

along with $\dot{T}_2 = 0$ on $x_1 = -L$ and $x_1 = L$, respectively, as well as the traction-free conditions $\dot{T}_1 = \dot{T}_2 = 0$ on $x_2 = -H/2$ and $x_2 = H/2$. The location x_0 of the neutral axis is determined

from the solution of the problem in order to ensure pure bending, i.e.

$$\int_{-H/2}^{H/2} \dot{T}_1 = 0 \quad (42)$$

on both $x_1 = -L$ and $x_1 = L$; see [3] for details of this procedure. Rigid body motion in the x_2 direction is again prevented by imposing $\dot{u}_2 = 0$ on the corner $(-L, -H/2)$. All calculations were performed using a loading/unloading rate $\dot{\theta} = \dot{\kappa}L = \pm 1000 \text{ s}^{-1}$, where $\dot{\kappa}$ is the imposed curvature rate.

3.4. Reference properties

In the calculations, the specimen aspect ratio was fixed at $2L/H = 3$ and the specimen sizes varied from $H = 1\text{--}8 \mu\text{m}$. The crystals were taken to be elastically isotropic with Young's modulus $E = 70 \text{ GPa}$ and Poisson's ratio $\nu = 0.33$. The materials had Frank–Read sources distributed on planes that were spaced $100b$ apart where $b = 0.25 \text{ nm}$ is the magnitude of Burger's vector of the edge dislocations in the calculations. Each source is randomly assigned a nucleation strength τ_{nuc} from a Gaussian distribution with average $\bar{\tau}_{\text{nuc}} = 50 \text{ MPa}$ and standard deviation $\Delta\tau_{\text{nuc}} = 1 \text{ MPa}$. The nucleation time for the sources t_{nuc} is 10 ns and the glide drag coefficient $B_g = 10^{-4} \text{ Pa s}$. Obstacles of strength $\tau_{\text{obs}} = 150 \text{ MPa}$ are also randomly distributed on planes spaced at $100b$ while the material-dependent annihilation distance $L_e = 6b$. The climb drag coefficient B_c is treated as a parameter whose sensitivity is investigated in this study and varied over the range $10^4 \leq B_c/B_g \leq \infty^3$. Most of the calculations are presented for either $B_c/B_g \leq \infty$ or $B_c/B_g = 10^4$; $B_c/B_g = \infty$ shall be referred to as the glide-only case while the cases with finite values of B_c shall be referred to as climb-assisted glide to emphasize the fact that even though the glide rates are significantly higher than the climb rates, dislocation climb assists in increasing the glide rates by enabling dislocations to bypass obstacles.

Crystals with two slip geometries are considered in this study: (i) crystals oriented for single slip with $\phi^{(1)} = 45^\circ$ and (ii) crystals with three slip systems oriented such that $\phi^{(1)} = 60^\circ$, $\phi^{(2)} = -60^\circ$ and $\phi^{(3)} = 90^\circ$. The sources and obstacles in the crystal had a density $\rho_{\text{src}} = 7 \mu\text{m}^{-2}$ and $\rho_{\text{obs}} = 14 \mu\text{m}^{-2}$, respectively, per slip system. Thus, the crystal with three slip systems had an overall source and obstacle density of $21 \mu\text{m}^{-2}$ and $42 \mu\text{m}^{-2}$, respectively. In order to reduce the statistical variations inherent in discrete dislocation calculations, all results presented here are averages over five realizations of sources and obstacles (i.e. different spatial distributions of the sources and obstacles but with the same overall density).

Since the (\sim) fields are given analytically, the finite element mesh needs to resolve the (\wedge) fields, but not the total fields. Thus, the element size is taken so as to resolve the (\wedge) field gradients. Typically, for the uniaxial tension and bending problems under consideration, wavelengths associated with the (\wedge) fields scale with the specimen size and thus in all the calculations, a uniform finite element grid was employed comprising of 120×80 bilinear quadrilaterals. This corresponds to a maximum element size of $0.0125 \mu\text{m}$ and $0.1 \mu\text{m}$ for the $H = 1 \mu\text{m}$ and $8 \mu\text{m}$ crystals, respectively. Mesh sensitivity studies were carried out on the $H = 2 \mu\text{m}$ crystals, and revealed that decreasing the mesh size by a factor of two had little effect on the numerical results presented subsequently. A time step of $\Delta t = 0.5 \text{ ns}$ was employed in all the calculations in order to adequately resolve the dislocation dynamics.

³ A dislocation climb rate that is 10^4 times lower compared with the glide rate might be unrealistic for diffusion-limited climb. For example, Bakó *et al* [26] argue that climb rates are 10 orders of magnitude smaller than glide rates at $T \approx 0.3T_m$. Here we illustrate the effects of climb over a wide range of climb rates and hence also use some accelerated rates in order to better illustrate the effects of dislocation climb.

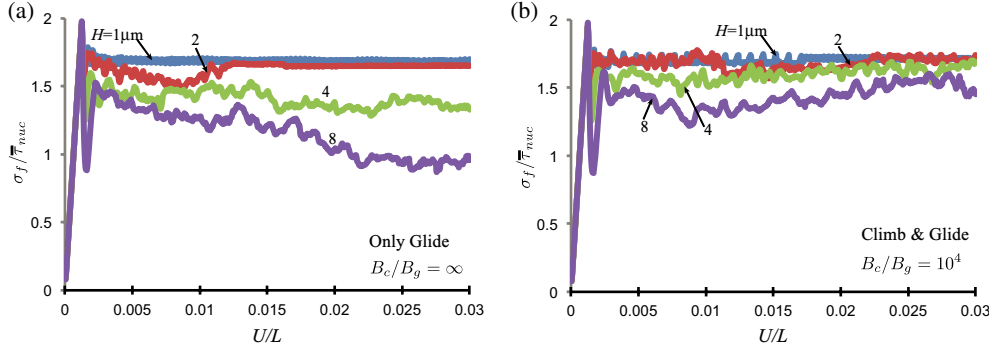


Figure 5. The normalized tensile stress $\sigma/\bar{\tau}_{\text{nuc}}$ versus strain U/L response of crystals with one active slip system. The response of crystals with glide-only ($B_c/B_g = \infty$) motion of dislocations is shown in (a) while in the case for climb-assisted glide ($B_c/B_g = 10^4$) is included in (b). Results are shown for four selected values of the specimen size H .

4. Crystals oriented for single slip

We first present results for crystals oriented such that only one slip system is active. This simple crystallographic orientation enables us to illustrate the effects of climb without the additional complications introduced by multiple slip systems. We then proceed to quantify the effect of multiple slip systems in section 5.

The two boundary value problems analysed are uniaxial tension and pure bending. Recall that while a macroscopic strain gradient is imposed in pure bending, the strain state is expected to be macroscopically uniform under imposed uniaxial tension. The imposed strain gradients in bending require the presence of geometrically necessary dislocations (GNDs) in addition to the statistically stored dislocations (SSDs) [27]. On the other hand, SSDs are expected to be predominant under uniaxial tension with no imposed strain gradients. The GND density is directly a consequence of the imposed strain gradients and hence not expected to be affected by dislocation climb. By contrast, the additional kinematic freedom provided to dislocations by dislocation climb should tend to allow the annihilation of a large fraction of the SSDs. Thus, dislocation climb is expected to have contrasting effects on the tensile and bending response of crystals. This is the primary reason for choosing these relatively simple but illustrative problems to demonstrate the effect of dislocation climb.

4.1. Uniaxial tension of crystals oriented for single slip

The applied nominal tensile stress σ is computed as

$$\sigma = -\frac{1}{H} \int_{-H/2}^{H/2} T_1(-L, x_2) dx_2 \quad (43)$$

to give the stress versus strain U/L response of the crystals. The predicted normalized stress $\sigma/\bar{\tau}_{\text{nuc}}$ versus U/L response of four specimen sizes are plotted in figures 5(a) and (b), respectively, for the glide-only ($B_c/B_g = \infty$) and climb-assisted glide case with $B_c/B_g = 10^4$. The corresponding predictions of the evolution of the dislocation density ρ are included in figure 6(a), where ρ is the areal density of the dislocations over the entire specimen area $2LH$.

First consider the glide-only case corresponding to $B_c/B_g = \infty$. In all the calculations, the first dislocation activity occurs at $\sigma/\bar{\tau}_{\text{nuc}} \approx 2$, since the Schmidt factor for the single available slip system is $(\sin 2\phi^{(1)}) = 0.5$. Subsequently, for the $H = 4$ and $8 \mu\text{m}$ specimens, there is a

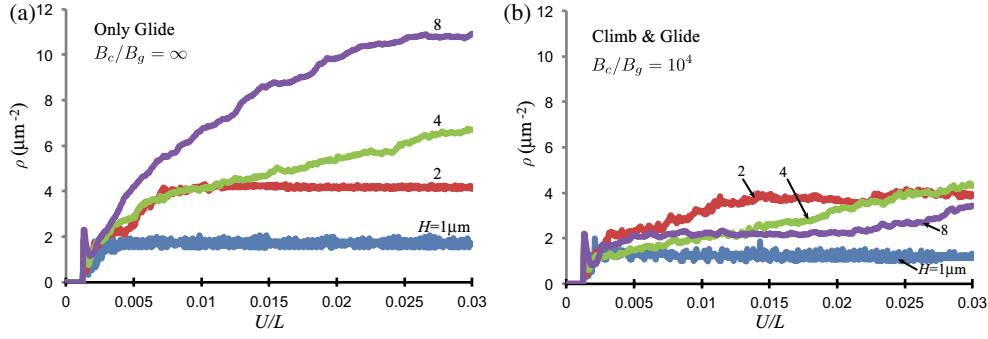


Figure 6. The evolution of the dislocation density ρ with imposed uniaxial strain U/L in the crystals with one active slip system corresponding to the tensile curves shown in figure 5. Results for (a) glide-only ($B_c/B_g = \infty$) motion of dislocations and (b) climb-assisted glide ($B_c/B_g = 10^4$) are included for four selected values of the specimen size H .

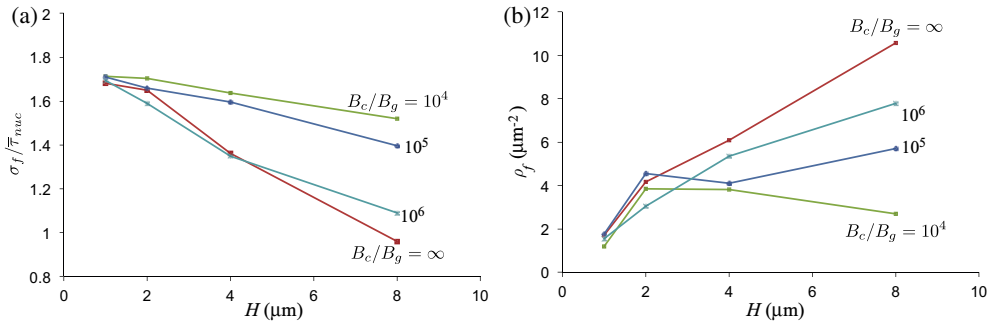


Figure 7. (a) The normalized flow strength $\sigma_f/\bar{\tau}_{nuc}$ and (b) the corresponding dislocation density ρ_f as a function of specimen size H for the crystal with one active slip system subjected to uniaxial tension. Results are shown for selected values of the climb to glide mobility ratio B_c/B_g .

sharp drop in the stress followed by essentially an ideally plastic response. On the other hand, there is nearly no stress drop in the $H = 1$ and $2 \mu\text{m}$ specimens with periodic fluctuations in the applied stress about a fixed mean value of the applied stress. In order to quantify the size dependence of the results we define the flow stress σ_f and the corresponding dislocation density ρ_f as the average values of σ and ρ , respectively, over the range $0.02 \leq U/L \leq 0.03$. These results are summarized in figures 7(a) and (b), where σ_f and ρ_f , respectively, are plotted as a function of the specimen size H : σ_f decreases with increasing H while ρ_f increases. These results are consistent with the dislocation starvation picture proposed by Greer *et al* [15] and confirmed in the calculations of Deshpande *et al* [5]. At small specimen sizes, the rate at which dislocations exit the specimen is approximately equal to the rate at which they are nucleated and hence very few dislocations are present in the specimen. This means that the stress state in the specimen is approximately uniform and a stress $\sigma = 2\bar{\tau}_{nuc}/\sin\phi^{(1)}$ needs to be applied to nucleate dislocations and get continued plastic flow. However, in the larger specimens, the rate of dislocation nucleation is greater than the rate at which dislocations exit the specimen and thus eventually a steady state is reached where a significant number of dislocations remain within the specimen: the stress concentrations associated with these dislocations enables continued nucleation of new dislocations at an applied stress below $2\bar{\tau}_{nuc}/\sin\phi^{(1)}$.

Next consider the case of climb-assisted glide with $B_c/B_g = 10^4$. The σ and ρ versus U/L responses plotted in figures 5(b) and 6(b), respectively, are seen to be significantly less

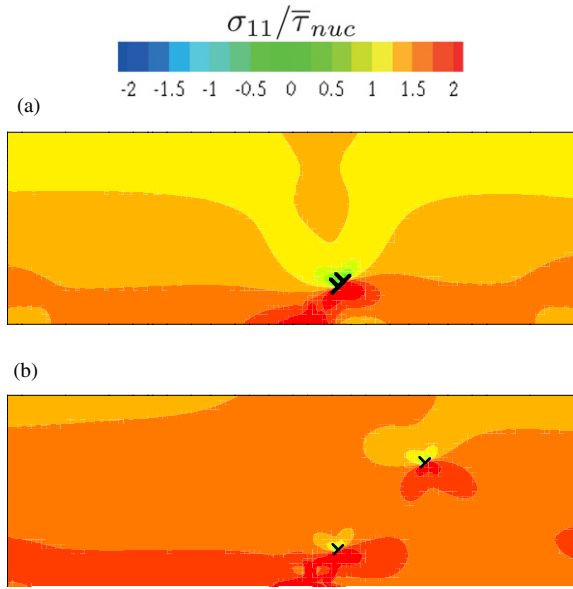


Figure 8. The dislocation structure and associated distribution of the normalized stress $\sigma_{11}/\bar{\tau}_{nuc}$ in the $H = 1 \mu\text{m}$ specimens subjected to uniaxial tension. Results are shown for the case of one active slip system with (a) glide-only and (b) climb-assisted glide ($B_c/B_g = 10^4$) motion of the dislocations.

sensitive to specimen size compared with the glide-only case and the corresponding dislocation densities are also significantly lower. Predictions of σ_f and ρ_f are summarized in figures 7(a) and (b), respectively, for selected values of B_c/B_g ranging from 10^4 to the glide-only case of $B_c/B_g = \infty$. In line with the discussion above, it is clear that the size dependence of σ_f reduces significantly with decreasing B_c/B_g . Moreover, the increased mobility of dislocations and their ability to bypass obstacles means that ρ_f is lower in the cases with a low B_c/B_g , especially in the larger specimens. The reduced size effect is then rationalized as follows. Climb plus glide motions of the dislocations allows dislocations to ‘climb’ around obstacles and break up any pile-ups that might otherwise be formed. Thus, dislocations can now more freely escape to the free surfaces which results in a low dislocation density for all specimen sizes considered here. This means that specimens of all sizes analysed here are starved of dislocations resulting in a negligible size effect. This also results in the counterintuitive result that the tensile strength of the large crystals is higher when climb is enabled (i.e. low values of B_c/B_g) compared with the reference glide-only case with $B_c/B_g = \infty$ (see figure 7(a)). We expect this to be an artefact of the assumptions that the glide mobility is unaffected by temperature as discussed further in section 6.

In order to illustrate the observation that dislocation starvation occurs in both the glide-only and the climb enabled cases in the small crystals while dislocation starvation only occurs in the larger crystals when climb is enabled, we plot in figures 8 and 9 the dislocation structures along with the normalized stress distribution $\sigma_{11}/\bar{\tau}_{nuc}$ at an applied strain $U/L = 0.03$. The $H = 1 \mu\text{m}$ crystals with $B_c/B_g = \infty$ and 10^4 are shown in figures 8(a) and (b), respectively, while the corresponding $H = 4 \mu\text{m}$ crystals are shown in figures 9(a) and (b). First consider the $H = 1 \mu\text{m}$ case. There are less than 10 dislocations present in the crystal for both values of B_c/B_g and the stress field within the crystals is approximately homogeneous consistent with the dislocation starvation picture. Next consider the $H = 4 \mu\text{m}$ case. It is clear that a

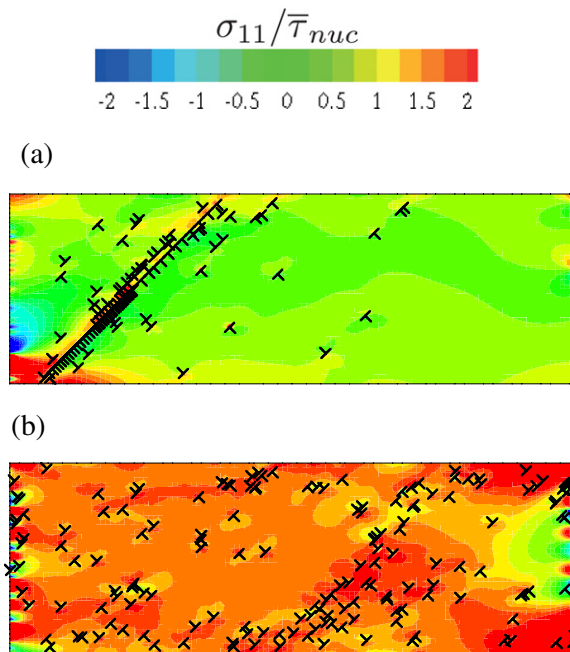


Figure 9. The dislocation structure and associated distribution of the normalized stress $\sigma_{11} / \bar{\tau}_{nuc}$ in the $H = 4 \mu\text{m}$ specimens subjected to uniaxial tension ($U/L = 0.03$). Results are shown for the case of one active slip system with (a) glide-only and (b) climb-assisted glide ($B_c/B_g = 10^4$) motion of the dislocations.

large pile-up is formed on a slip plane in the $B_c/B_g = \infty$ case as dislocations get pinned at an obstacle. The dislocations in this pile-up capture dislocations on adjacent planes creating a high local dislocation density with a strong inhomogeneity in the stress field in the vicinity of this cluster of dislocations. On the other hand, there are significantly fewer dislocations that are evenly distributed throughout the crystal in the $B_c/B_g = 10^4$ case. Furthermore, the stress field too is more homogeneous indicating that this crystal is in the dislocation starvation regime.

The deformed configurations at an applied strain $U/L = 0.03$ of the $H = 4 \mu\text{m}$ crystals are illustrated in figures 10(a) and (b) for the glide-only ($B_c/B_g = \infty$) and climb-assisted glide ($B_c/B_g = 10^4$) cases, respectively. The deformed configurations are plotted using the FE mesh used in the DDP calculations with the deformations magnified by a factor of five. Note that these meshes are only used to illustrate the deformations and the intense localizations seen do not result in numerical difficulties as in continuum plasticity calculations: in DDP the FE calculations are only used to calculate the smooth ($\hat{\cdot}$) fields that correct the boundary conditions. On comparing figures 10(a) and (b) it is clear that while large surface steps due to localized slip form in the glide-only case, deformation is much more distributed in the climb-assisted glide case. This is consistent with recent observations on the compression of micro-pillars. Room temperature compression of Ni and Ni₃Al single crystal micro-pillars by Uchic *et al* [16] (dislocation motion at room temperature in Ni and Ni₃Al is expected to primarily occur by dislocation glide) results in the formation of large surface steps. By contrast, Lee *et al* [13] observed that the surface of the deformed Indium micro-pillars was relatively smooth when those were subjected to room temperature compression (Indium at room temperature is in the power-law creep regime with climb-assisted glide expected to

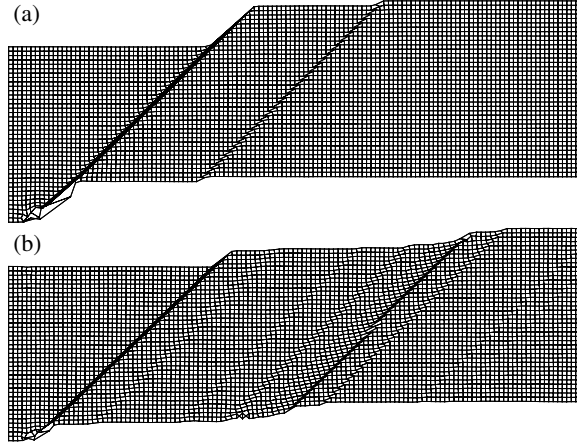


Figure 10. The deformed configurations of the $H = 4 \mu\text{m}$ specimens with one active slip system subjected to uniaxial tension. The deformations at an applied $U/L = 0.03$ are illustrated on the FE meshes with the deformations magnified by a factor of five for (a) glide-only and (b) climb-assisted glide ($B_c/B_g = 10^4$) motion of the dislocations.

be the primary mechanism of dislocation motion). Furthermore, Lee *et al* [13] observed a significantly smaller size effect of the compressive strength of Indium compared with the size effect observed in Ni and Ni₃Al by Uchic *et al* [16]. The results presented here are consistent with these observations and provide a possible explanation of the underlying mechanisms.

4.2. Bending of crystals oriented for single slip

The applied bending moment is calculated as

$$M = \int_{-H/2}^{H/2} x_2 T_1(L, x_2) dx_2, \quad (44)$$

while the curvature κ is related to the applied end rotations θ via the relation $\kappa \equiv \theta/L$. Predictions of the normalized moment M/M_{ref} versus normalized applied curvature $\kappa H/2$ curves are included in figures 11(a) and (b) for the glide-only ($B_c/B_g = \infty$) and $B_c/B_g = 10^4$ cases, respectively. In each case results are shown for four values of the specimen size H . The normalization moment M_{ref} is defined as

$$M_{\text{ref}} = \frac{2}{H} \int_{-H/2}^{H/2} \bar{\tau}_{\text{nuc}} x_2^2 dx_2 = \frac{2}{3} \bar{\tau}_{\text{nuc}} \left(\frac{H}{2} \right)^2, \quad (45)$$

corresponding to the moment for a linear stress distribution $2\bar{\tau}_{\text{nuc}}x_2/H$. The normalizations of the moment and curvature in figure 11 are chosen so as to give a unique curve for a size-independent material response.

First consider the glide-only case, shown in figure 11(a). Following an initial elastic response, the first dislocation activity occurs at $M/M_{\text{ref}} \approx 2$ in all cases. The subsequent response is strongly size dependent with the $H = 1 \mu\text{m}$ displaying a strongly hardening response while the $H = 8 \mu\text{m}$ crystal displays a mildly softening response. This size effect is summarized in figure 12 where the normalized average moment M_f/M_{ref} (M_f is defined as the average applied moment over the range $0.004 \leq \kappa H/2 \leq 0.005$) and the corresponding average dislocation density ρ_f are included as a function of the specimen size H . Both M_f and ρ_f increase with decreasing H . This increase in both bending strength and dislocation

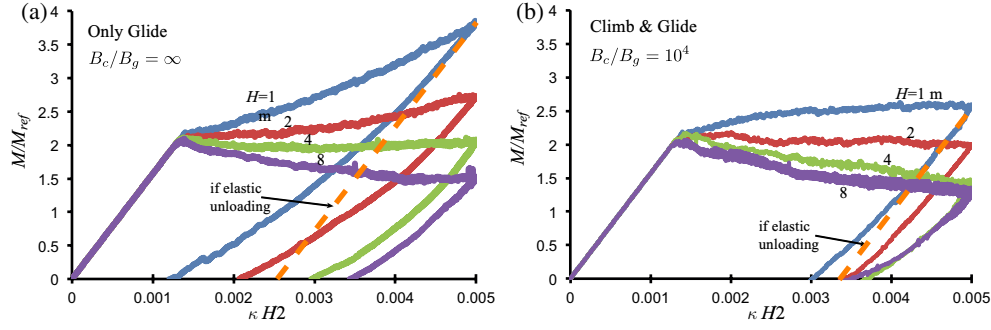


Figure 11. The normalized bending moment M/M_{ref} versus applied normalized curvature $\kappa H/2$ response of crystals with one active slip system. The response of crystals with glide-only ($B_c/B_g = \infty$) motion of dislocations is shown in (a) while in the case for climb-assisted glide ($B_c/B_g = 10^4$) is included in (b). Results are shown for four selected values of the specimen size H .

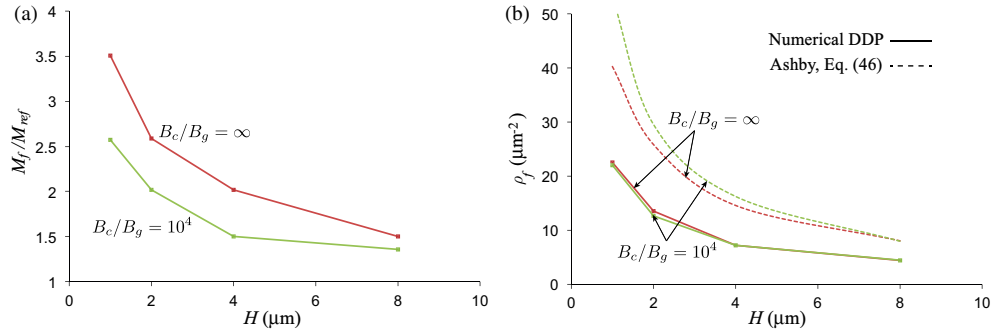


Figure 12. (a) The normalized flow moment M_f/M_{ref} and (b) the corresponding dislocation density ρ_f as a function of specimen size H for the crystal with one active slip system subjected to pure bending. Results are shown for both the glide-only ($B_c/B_g = \infty$) and climb-assisted glide case of $B_c/B_g = 10^4$. In (b) the predictions of the GND density, equation (46), are included.

density with decreasing size is consistent with the DDP predictions of Cleveringa *et al* [3]. The predicted size effect is attributed to the presence of GNDs whose density increases with decreasing specimen. Ashby [27] developed a simple analytical expression for the GND density of a nominally isotropic plastic material subjected to bending given by

$$\rho_f^{\text{Ashby}} = \frac{\kappa_p}{b}, \quad (46)$$

where κ_p is the plastic curvature that is related to the applied total curvature κ via

$$\kappa_p = \kappa - \kappa_e. \quad (47)$$

The elastic curvature κ_e at an applied moment M is $\kappa_e = 12M(1 - \nu^2)/EH^3$. The prediction based on the Ashby [27] formula is included in figure 12(b): while the qualitative trend for the variation of ρ_f with H is captured by the equation (46), the formula predicts a higher dislocation density compared with the DDP simulations. This discrepancy was also reported by Cleveringa *et al* [3] and is attributed to the fact that the Ashby [27] formula assumes a plastically isotropic material while the crystal employed in the DDP calculations reported here is highly anisotropic with only one slip system.

Now consider the case of climb-assisted glide with $B_c/B_g = 10^4$. Again, deviation from the linear elastic curves of the normalized moment M/M_{ref} versus $\kappa H/2$ curves first

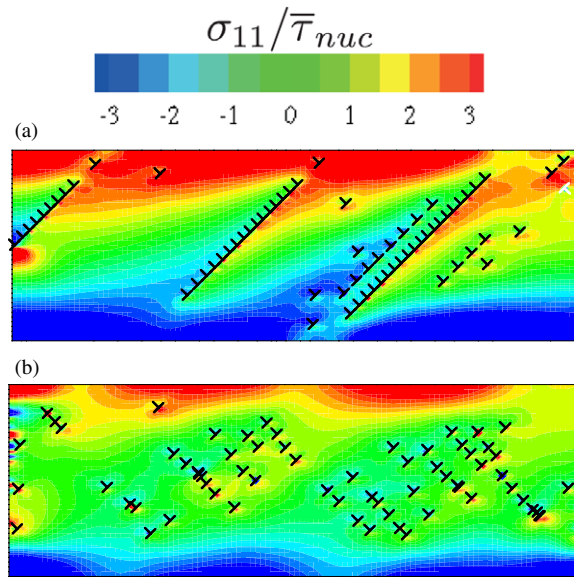


Figure 13. The dislocation structure and associated distribution of the normalized stress $\sigma_{11}/\bar{\tau}_{nuc}$ in the $H = 1 \mu\text{m}$ specimens subjected to pure bending ($\kappa H/2 = 0.005$). Results are shown for the case of one active slip system with (a) glide-only and (b) climb-assisted glide ($B_c/B_g = 10^4$) motion of the dislocations.

occurs at $M/M_{ref} \approx 2$. While the subsequent response displays some size sensitivity, this size dependence is significantly less than in the glide-only case. In fact, the response of the $H = 1 \mu\text{m}$ crystal is nearly ideally plastic while the $H = 8 \mu\text{m}$ crystal displays a softening response over the range of κ computed here. The corresponding predictions of M_f and ρ_f (using the same definitions as in the glide-only case) are included in figures 12(a) and (b), respectively. Intriguingly, while ρ_f in the glide-only and climb-assisted glide cases are nearly identical, the bending strength M_f of the crystals with climb-assisted glide is significantly less than in the glide-only case, especially at small values of H . We proceed to try and understand these apparently conflicting results.

Contours of the normalized bending stress $\sigma_{11}/\bar{\tau}_{nuc}$ along with the associated dislocation structures at $\kappa H/2 = 0.005$ in the $H = 1 \mu\text{m}$ crystal are included in figures 13(a) and (b), for the glide-only and climb-assisted glide case ($B_c/B_g = 10^4$), respectively. Two key observations can be made: (i) there is a significantly larger boundary layer of higher stresses near the top and bottom surfaces of the crystal with glide-only dislocation motion and (ii) while lines of dislocation pile-ups along the $\phi^{(1)} = 45^\circ$ slip planes form in the glide-only case, lower energy dislocation wall structures form perpendicular to the active slip system in the climb-assisted glide case. Thus, even though the dislocation densities in both cases are nearly identical, the dislocation wall structures that form in the climb-assisted glide case store significantly less elastic energy and this results in the reduced hardening and size effects compared with the glide-only case.

These differences in the dislocation structures in the glide-only and climb-assisted glide cases also manifest themselves in the unloading response of the crystals included in figure 11. Some reverse plasticity is observed in both glide-only and climb-assisted glide cases and we

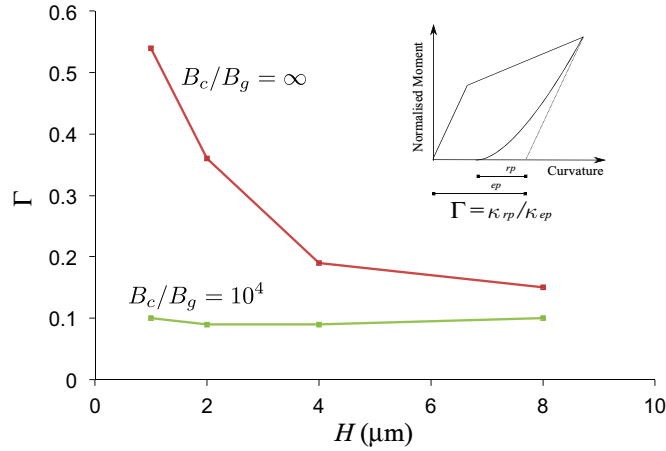


Figure 14. The reverse plastic deformation as quantified via the measure Γ as a function of the specimen size H in the specimens with one active slip system subjected to pure bending. Results are shown for both the glide-only and climb-assisted glide ($B_c/B_g = 10^4$) cases for unloading from $\kappa H/2 = 0.005$. The definition of Γ is illustrated in the inset.

quantify this using the non-dimensional measure Γ defined as

$$\Gamma \equiv \frac{\kappa_{rp}}{\kappa_{ep}}, \quad (48)$$

where κ_{rp} and κ_{ep} are defined in the inset in figure 14. Pure elastic unloading corresponds to $\kappa_{rp} = 0$ while reverse plasticity that results in unloading such that $M = 0$ when $\kappa = 0$ gives the other limit of $\kappa_{rp} = \kappa_{ep}$. Thus, the non-dimensional measure Γ varies between 0 and 1 with higher values of Γ signifying high levels of reverse plasticity or kinematic hardening. Predictions of Γ as a function of the specimen size H are included in figure 14 for both the glide-only and the climb-assisted glide case with $B_c/B_g = 10^4$ for unloading from $\kappa H/2 = 0.005$. Reverse plasticity (and Γ) is seen to dramatically increase with decreasing H for the glide-only case due to the formation of the high energy dislocation structures as seen in figure 13(a). On the other hand, Γ remains approximately constant at a relatively low value of $\Gamma \approx 0.1$ over the full range of sizes analysed here for the climb-assisted glide case with $B_c/B_g = 10^4$. This can be traced back to the fact that the dislocation wall structures are relatively low energy structures which give rise to minimal kinematic hardening.

5. Crystals with three active slip systems

In this section, we present selected results for crystals with three active slip systems ($\phi^{(1,2)} = \pm 60^\circ$ and $\phi^{(3)} = 90^\circ$) subjected to simple tension and pure bending loading conditions. The aim here is to highlight the differences between single and multiple slip rather than investigate the response of crystals with multiple slip systems in an exhaustive manner. Hence results for the climb-assisted glide case are only shown for the reference value of $B_c/B_g = 10^4$.

Predictions of the variation of the tensile flow strength σ_f and the corresponding average dislocation density ρ_f are plotted in figures 15(a) and (b), respectively. Unlike in the single slip case, a significant size effect is observed in both the glide-only and climb-assisted glide cases with σ_f decreasing with increasing H . In fact, the tensile flow strength in both the glide-only and climb-assisted glide cases are nearly indistinguishable over the whole range of

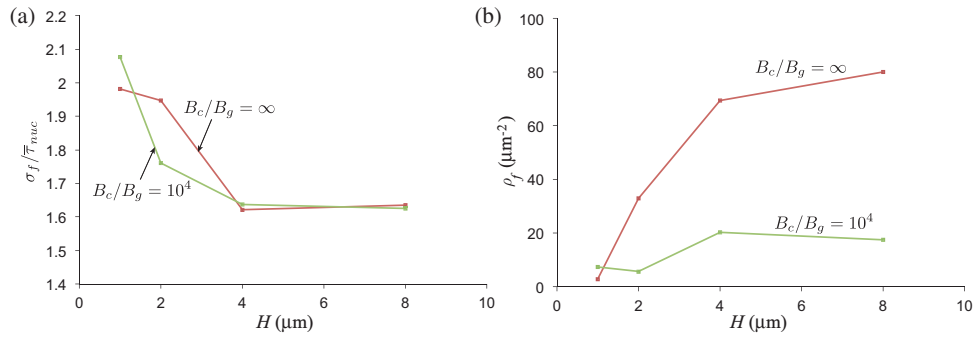


Figure 15. (a) The normalized flow strength $\sigma_f / \bar{\tau}_{nuc}$ and (b) the corresponding dislocation density ρ_f as a function of specimen size H for the crystal with three active slip system subjected to uniaxial tension. Results are shown for both the glide-only ($B_c/B_g = \infty$) and climb-assisted glide case of $B_c/B_g = 10^4$.

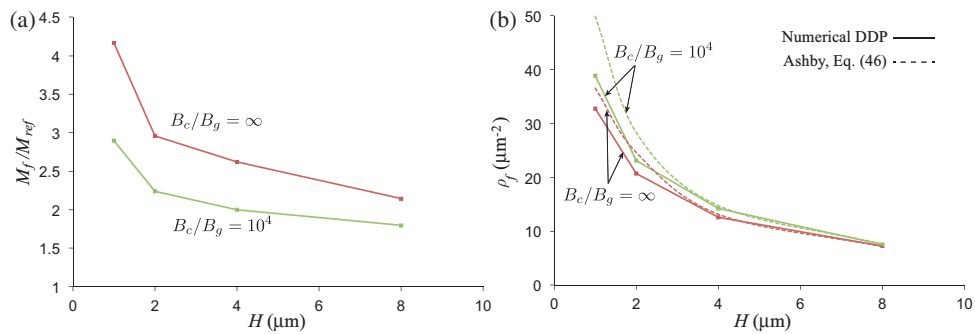


Figure 16. (a) The normalized flow moment M_f / M_{ref} and (b) the corresponding dislocation density ρ_f as a function of specimen size H for the crystal with three active slip system subjected to pure bending. Results are shown for both the glide-only ($B_c/B_g = \infty$) and climb-assisted glide case of $B_c/B_g = 10^4$. In (b) the predictions of the GND density, equation (46), are included.

specimen sizes considered here. By contrast, while ρ_f increases with increasing H in both the glide-only and climb-assisted glide cases, the dislocation densities are significantly lower when dislocations are permitted to climb. However, a comparison with figure 7(b) illustrates that even when climb is permitted the dislocation densities are significantly higher in the multiple slip case compared with when only one slip system is active. Thus, unlike in the single slip case, dislocation starvation does not occur in the larger specimens with multiple active slip systems even though dislocation motion is by climb-assisted glide.

Predictions of the normalized average moment M_f / M_{ref} and the average dislocation density ρ_f as a function of specimen size H are included in figures 16(a) and (b), respectively. The results are in line with the single slip case, namely, while the dislocation density is unaffected by dislocation climb, the size dependence of the bending strength of the crystal is considerably reduced compared with the glide-only case. The reasons for this are similar to the single slip case; namely, climb permits dislocations to re-arrange themselves in lower energy configurations. This is clearly seen in figures 17(a) and (b) where contours of the normalized bending stress $\sigma_{11} / \bar{\tau}_{nuc}$ are plotted along with the predicted dislocation structure in the $H = 1 \mu\text{m}$ specimen at an applied $\kappa H/2 = 0.005$ for the glide-only and climb-assisted glide cases, respectively. Again, climb is seen to break-up the dislocation pile-ups and form low energy wall structures. However, a comparison with figure 13 clearly shows that the

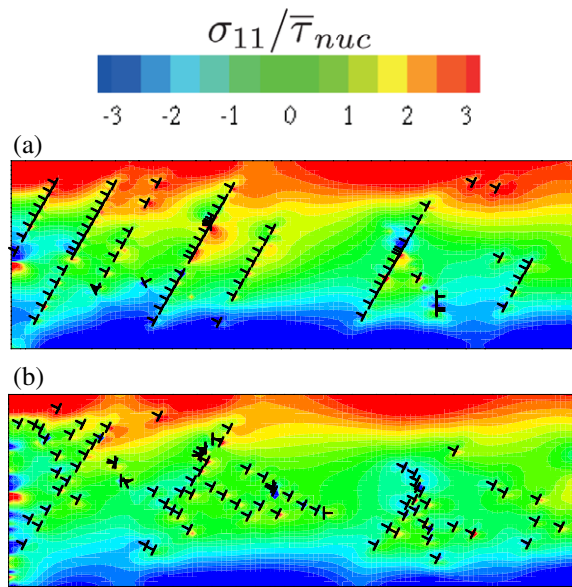


Figure 17. The dislocation structure and associated distribution of the normalized stress $\sigma_{11} / \bar{\tau}_{nuc}$ in the $H = 1 \mu\text{m}$ specimens subjected to pure bending ($\kappa H/2 = 0.005$). Results are shown for the case of three active slip systems with (a) glide-only and (b) climb-assisted glide ($B_c/B_g = 10^4$) motion of the dislocations.

dislocation density is considerably higher in these crystals with multiple active slip systems. In fact, the DDP predictions of the dislocation density are now in excellent agreement with the Ashby [27] formula (equation (46)) as the crystal with multiple slip systems is nearly plastically isotropic.

6. Discussion

The simulations for climb-assisted dislocation glide presented here pertain to plasticity at elevated temperatures when dislocation climb rates become appreciable. However, a number of temperature-dependent mechanisms have been neglected in these analysis in order to emphasize and clarify the role of dislocation climb. Notably as discussed by Frost and Ashby [28], dislocation glide is a kinetic process with the average velocity of dislocations determined almost entirely by their waiting time at obstacles. In particular, there are two broad class of obstacles: discrete obstacles which are bypassed individually by a moving dislocation (e.g. precipitates) or cut by it (e.g. forest dislocations or weak precipitates); and extended, diffuse barriers to dislocation motion which are overcome collectively (e.g. lattice friction). Dislocations require to acquire certain activation energy to overcome either of these obstacles which results in an Arrhenius type temperature dependence of the average dislocation velocities: the often observed reduction in the yield strength with increasing temperature is attributed to the enhanced dislocation velocities at higher temperatures. We note from figure 5 that the tensile strength of the crystals with climb-assisted dislocation glide is approximately equal to the crystals wherein dislocation motion is by glide-only. Thus, the calculations do not predict the reduction in strength that is typically observed at high temperatures when dislocation climb is active. This is primarily due to the fact that we have kept both the glide drag coefficient B_g and the obstacle strength τ_{obs} fixed in all the simulations presented here.

Therefore, the effective glide velocities of the dislocations remain unchanged between the glide-only and climb-assisted glide cases resulting in σ_f being insensitive to the ratio B_c/B_g . We note in passing that a temperature-dependent obstacle strength and glide drag coefficient can easily be incorporated within the DDP framework employed here.

The results presented here demonstrate that climb has contrasting effects in specimens subjected to uniaxial tension or pure bending. Consider the case of crystals with three active slip systems (there are some subtle differences when only one slip system is active but the multiple slip system case is more relevant from a practical perspective). Climb is shown to have a negligible effect on the tensile stress versus strain response of these crystals although the dislocation density when climb is enabled is significantly lower due to the ability of dislocations to bypass obstacles by climb. The dislocations in these crystals under tensile loading are primarily statistical in nature and the density of the statistical dislocations does not significantly affect the predicted strengths in these 2D discrete dislocation calculations (recall that Taylor [29] hardening effects are not included in these calculations). By contrast, dislocation climb significantly reduces the size effect of the bending strength M_f of the crystals even though the dislocation densities in the glide-only and climb-assisted glide cases are nearly identical; see figure 16(b). The imposed strain gradients in bending require the presence of GNDs: the results here suggest that most of the dislocations are GNDs and hence their densities are unaffected by permitting dislocations to climb. However, the additional kinematic freedom permitted by dislocation climb allows dislocations to form lower energy wall structures compared with the pile-ups in the glide-only case; compare figures 17(a) and (b). This results in significantly lower hardening in the climb-assisted glide case which results in the reduced size effect. These predictions are supported by recent indentation size effect measurements in Copper for temperatures ranging from ambient to 200 °C by Franke *et al* [17]. Similar to bending, the indentation size effect is also primarily attributed to the GND effect and Franke *et al* [17] demonstrated that the indentation size effect is reduced considerably with increasing temperature.

7. Concluding remarks

A new framework for incorporating dislocation climb in addition to dislocation glide into a two-dimensional discrete dislocation plasticity (DDP) framework to solve boundary value problems is presented here. The climb velocity of the dislocations is shown to be governed by a drag-type relation for both diffusion-limited and sink-limited vacancy kinetics. A key difference between glide-only motion of dislocations and climb plus glide motion of dislocations is that the deformation state of the body cannot be constructed from only the knowledge of the current positions of the dislocations. The small-strain DDP problem was solved using a rate formulation with the displacement rate fields due to the motion of the dislocations calculated by accounting for both the climb and glide motions of the dislocations.

Predictions of this formulation are illustrated using two simple problems, namely, uniaxial tension and pure bending. Results are presented for cases where there is only one active slip system as well as for cases with three active slip systems. First consider the case of single slip. When dislocation motion is by climb-assisted glide, the ability of dislocations to bypass obstacles results in low dislocation densities for all specimen sizes under uniaxial loading conditions. This results in dislocation starvation for all specimens sizes considered here and only a small size effect in the tensile strength. By contrast, when dislocation motion is only by glide, dislocation starvation occurs only in the smaller specimens resulting in a pronounced size effect with the tensile strength reducing with increasing specimen size. These predictions thus provide a possible explanation for the absence of a size effect for the room

temperature compressive strength of Indium as observed by Lee *et al* [13] in contrast to the strong size effect observed in Ni by Uchic *et al* [16]. Under pure bending loading conditions, geometrically necessary dislocations (GNDs) dominate and the dislocation densities in both the climb-assisted glide and glide-only cases are nearly identical. Also, the GNDs result in the normalized bending strength increasing with decreasing specimen size. The additional kinematic freedom available to dislocations when climb is enabled allows them to re-arrange in wall structures that have a significantly lower elastic energy compared with the dislocation pile-up structures that form in the glide-only case. This results in a significantly reduced bending size effect in the climb-assisted glide case. Recent high temperature indentation hardness measurements by Franke *et al* [17] show that the plasticity size effect related to GNDs is reduced with increasing temperature. While there are numerous thermally activated processes that can result in the change in the intrinsic material length scale with increasing temperature, climb motion of dislocations is one such process. The climb-assisted glide DDP framework presented here suggests that dislocation climb can give rise to this reduced plasticity size effect by allowing dislocations to rearrange themselves into lower energy structures. The response of crystals with multiple active slip systems is qualitatively similar to the case of single slip with one key difference. With the increased number of dislocation sources, dislocation starvation does not occur even in the climb-assisted glide case over the entire range of specimen sizes considered here.

Acknowledgments

Part of this work was carried out when KD was visiting the Engineering Department of Cambridge University and he kindly acknowledges support during that period.

References

- [1] Van der Giessen E and Needleman A 1995 Discrete dislocation plasticity: a simple planar model *Modelling Simul. Mater. Sci. Eng.* **3** 689–735
- [2] Cleveringa H H M, Van der Giessen E and Needleman A 1997 Comparison of discrete dislocation and continuum plasticity predictions for a composite material *Acta Mater.* **45** 3163–79
- [3] Cleveringa H H M, Van der Giessen E and Needleman A 1999 A discrete dislocation analysis of bending *Int. J. Plasticity* **15** 837–68
- [4] Balint D S, Deshpande V S, Needleman A and Van der Giessen E 2006 Discrete dislocation plasticity analysis of the wedge indentation of films *J. Mech. Phys. Solids* **54** 2281–303
- [5] Deshpande V S, Needleman A and Van der Giessen E 2005 Plasticity size effects in tension and compression of single crystals *J. Mech. Phys. Solids* **53** 2661–91
- [6] Danas K, Deshpande V S and Fleck N A 2010 The role of surface coatings in size effects: discrete dislocations vs. strain-gradient crystal plasticity *Inter. J. Plasticity* **26** 1792–1805
- [7] Cleveringa H H M, Van der Giessen E and Needleman A 2000 A discrete dislocation analysis of mode I crack growth *J. Mech. Phys. Solids* **48** 1133–57
- [8] Cleveringa H H M, Van der Giessen E and Needleman A 2002 Discrete dislocation modeling of fatigue crack propagation *Acta Mater.* **50** 831–46
- [9] Fivel M C and Canova G R 1999 Developing rigorous boundary conditions to simulations of discrete dislocation dynamics *Modelling Simul. Mater. Sci. Eng.* **7** 753–68
- [10] Benzerga A A, Brechet Y, Needleman A and Van der Giessen E 2004 Incorporating three-dimensional mechanisms into two-dimensional dislocation dynamics *Modelling Simul. Mater. Sci. Eng.* **12** 159–96
- [11] Arzt E 1998 Size effects in materials due to micro-structural and dimensional constraints: a comparative review *Acta Mater.* **46** 5611–26
- [12] Brown L 1997 Transition from laminar to rotational motion in plasticity *Phil. Trans. R. Soc. A* **355** 1979–90
- [13] Lee G, Kim J-Y, Burek M J, Greer J R and Tsui T Y 2011 Plastic deformation of indium nanostructures *Mater. Sci. Eng. A* **528** 6112–20

- [14] Greer J and De Hosson J 2011 Review: plasticity in small-sized metallic systems: intrinsic versus extrinsic size effect *Prog. Mater. Sci.* **56** 654–724
- [15] Greer J R, Oliver W C and Nix W D 2005 Size dependence of mechanical properties of gold at the micron scale in the absence of strain gradients *Acta Mater.* **53** 1821–30
- [16] Uchic M, Dimiduk D, Florando J and Nix W 2004 Sample dimensions influence strength and crystal plasticity *Science* **305** 986–9
- [17] Franke O, Trenkle J C and Schuh C A 2010 Temperature dependence of the indentation size effect *J. Mater. Res.* **25** 1225–9
- [18] Mordehai D, Clouet E, Fivel M and Verdier M 2008 Introducing dislocation climb by bulk diffusion in discrete dislocation dynamics *Phil. Mag.* **88** 899–925
- [19] Xiang Y and Srolovitz D J 2006 Dislocation climb effects on particle bypass mechanisms *Phil. Mag.* **86** 3937–57
- [20] Bakó B, Groma I, Györgyi G and Zimányi G 2006 Dislocation patterning: the role of climb in meso-scale simulations *Comput. Mater. Sci.* **38** 22–8
- [21] Balluffi R W, Allen S M and Carter W C 2005 *Kinetics of Materials* (Hoboken, NJ: Wiley)
- [22] Gao Y and Cocks A C F 2009 Thermodynamic variation approach for climb of an edge dislocation *Acta Mech. Solida Sin.* **22** 426–35
- [23] Hirth J P and Lothe J 1968 *Theory of Dislocations* (New York: McGraw-Hill)
- [24] Ham F S 1959 Stress-assisted precipitation on dislocations *J. Appl. Phys.* **30** 915–26
- [25] Kubin L P, Canova G, Condat M, Devincere B, Pontikis V and Bréchet Y 1992 Dislocation microstructures and plastic flow: a 3D simulation *Solid State Phenom.* **23–24** 455–72
- [26] Bakó B, Clouet E, Dupuy L and Bletry M 2011 Dislocation dynamics simulations with climb: kinetics of dislocation loop coarsening controlled by bulk diffusion *Philos. Mag.* **91** 3173–91
- [27] Ashby M F 1970 The deformation of plastically non-homogeneous materials *Philos. Mag.* **21** 399–424
- [28] Frost H and Ashby M 1982 *Deformation-mechanism Maps: the Plasticity and Creep of Metals and Ceramics* (New York: Pergamon Press)
- [29] Taylor G I 1938 Plastic strain in metals *J. Inst. Met.* **62** 307–324